# Experimental study of the $^{11,12}$B$(n,\gamma)$ reactions and their influence on $r$-process nucleosynthesis of light elements

H. Y. Lee,[*] J. P. Greene, C. L. Jiang, R. C. Pardo, K. E. Rehm, and J. P. Schiffer
*Physics Division, Argonne National Laboratory, Argonne, Illinois 60439, USA*

A. H. Wuosmaa, N. J. Goodman, J. C. Lighthall, and S. T. Marley
*Department of Physics, Western Michigan University, Kalamazoo, Michigan 49008, USA*

K. Otsuki[†]
*Gesellschaft für Schwerionenforschung, D-64291 Darmstadt, Germany*

N. Patel
*Department of Physics, Colorado School of Mines, Golden, Colorado 80401, USA*

M. Beard, M. Notani, and X. D. Tang
*Department of Physics & The Joint Institute for Nuclear Astrophysics, University of Notre Dame, Notre Dame, Indiana 46556, USA*

We have studied the neutron-transfer reactions $^{11,12}$B$(d,p)^{12,13}$B in inverse kinematics to obtain information about the neutron-capture reactions $^{11,12}$B$(n,\gamma)$. These capture reactions are suggested to play a role in seeding $r$-process nucleosynthesis through the production of light, neutron-rich nuclei. The neutron spectroscopic factors of the states in $^{12,13}$B were deduced and the branching ratio of the neutron-unbound state at $E_X = 3.389$ MeV in $^{12}$B was obtained to provide the ratio of partial widths, $\Gamma_n/\Gamma_\gamma$. The reaction rates for $^{11,12}$B$(n,\gamma)$ are estimated for direct captures and resonant captures and compared with previous compilations. The astrophysical implications, especially for neutrino-driven wind models in core-collapse supernovae, are discussed in the $r$-process network framework using our updated reaction rates.

PACS number(s): 26.30.−k, 25.40.Lw, 82.20.Pm

## I. INTRODUCTION

The determination of the possible astrophysical site and understanding the mechanism of heavy-element production are important problems in $r$-process nucleosynthesis. Because of the predicted high neutron flux and temperature, it has been suggested that the $r$-process occurs in explosive environments. Observational studies [1,2] revealed that $r$-process elements heavier than Ba show the same abundance pattern in dozens of metal-poor stars with [Fe/H] $> -3$.[1]

This pattern also coincides with that of the solar $r$-process that is obtained by subtracting the theoretically predicted $s$-process contribution from the observed solar abundances. These observational facts suggest that the $r$-process for those heavy elements is probably a primary process. The neutrino-driven wind from proto-neutron stars in Type II supernovae [3–5], neutron star mergers [6], and neutron-rich jets from supernovae [7–9] and following $\gamma$-ray bursts [10,11] have been intensively studied as plausible sites.

Neutrino-driven winds or hot bubble models in core-collapse supernovae [5] are expected to generate the high temperature and entropy regions outside the proto-neutron star via neutrino-nucleus interactions. Under the high entropy condition produced by neutrino heating, iron group nuclei formed from prior quiescent burnings disintegrate into neutrons and protons, which then start coalescing to form $\alpha$ particles as the adiabatic expansion of the wind cools the star further. With abundant $\alpha$ particles, seed nuclei with $70 \leqslant A \leqslant 120$ are reassembled until the temperature becomes too low to overcome the Coulomb barriers, a process referred to as the $\alpha$-process. A previous study of the importance of the role of the $\alpha$-process in $r$-process nucleosynthesis [12] showed that a different abundance distribution of heavy elements can be obtained by including the excess neutron flux during the early reassembly of $\alpha$ particles. The large mass fraction of neutrons and $\alpha$ particles could then enhance the formation of $^{12}$C through the reaction chain of $\alpha(\alpha n,\gamma)^9$Be$(\alpha,n)^{12}$C by a factor of 10 compared to the usual triple-$\alpha$ reaction solely, whose rate declines slowly for $T_9 > 1$.

In particular, the neutrino-driven wind model in gravitational core-collapse Type II supernovae with a short dynamic time scale of the expanding wind [13,14] produces fewer seed nuclei, yielding more neutrons available to be captured on light, neutron-rich nuclei. This increase results in a higher ratio of neutrons to seed nuclei, suggesting a promising site for $r$-process nucleosynthesis.

Most of these $r$-process studies have considered neutron captures on many ($\sim$6000) heavy nuclei and a limited number of light nuclei. Recent efforts [14,15] to understand the wind

_____

[*]hylee@lanl.gov; present address: LANSCE-NS, Los Alamos National Laboratory, NM 87545, USA.

[†]Present address: Faculty of Sciences, Hokkaido University, Sapporo 060-0810, Japan.

[1][Fe/H] $= \log_{10}$(Fe/H)$_{\text{star}} - \log_{10}$(Fe/H)$_{\text{Sun}}$.

models, however, have demonstrated the influence on the final abundance of $r$-process nuclei from neutron captures on light, neutron-rich nuclei. Terasawa *et al.* [14] studied new reaction paths by extending their network to include 40 more neutron-rich nuclei with $Z < 10$. Under the same astrophysical conditions, these additional neutron-rich nuclei create extra paths to reach the carbon-isotope seeds through the Be chain, $\alpha(\alpha n, \gamma)^9\text{Be}(n, \gamma)^{10}\text{Be}(\alpha, \gamma)^{14}\text{C}$, and the Li-B chain, $\alpha(t, \gamma)^7\text{Li}(n, \gamma)^8\text{Li}(\alpha, n)^{11}\text{B}$, followed by successive neutron captures on boron isotopes until $^{15}\text{B}$ $\beta$ decays to $^{15}\text{C}$. This comparison demonstrated differences in the final $r$-process abundances of heavy elements produced by these additional paths, in some cases by a factor of 10. Following this, Sasaqui *et al.* [15] have quantified the uncertainty of $r$-process nucleosynthesis, especially studying the dependence of the sensitivities among 18 light, neutron-rich elements under different explosive environments.

Unfortunately, most reaction rates for neutron-rich radioactive nuclei are still unmeasured or poorly known experimentally in the temperature range of $T_9 < 2$. Although neutron capture is one of the most important reactions in different astrophysical models, it cannot be studied directly in the laboratory with short-lived radioactive targets. Some of the relevant information can be obtained indirectly through the study of neutron-transfer reactions. To better understand $(n, \gamma)$ reaction rates from $(d, p)$ measurements, we have studied the $(d, p)$ reaction on the boron isotopes $^{11}\text{B}$ and radioactive $^{12}\text{B}$.

Rauscher *et al.* [16] estimated the uncertainties of the reaction rates for the $^{11}\text{B}(n, \gamma)$ and $^{12}\text{B}(n, \gamma)$ reactions to be at least a factor of 2, based on the limited spectroscopic information on $^{12,13}\text{B}$ and by considering direct and resonant captures. Although there have been several investigations of the structure of $^{13}\text{B}$ [17,18], such as single-nucleon knockout [19], a proton intruder study [20], and a search for isobaric analog states [21], as well as theoretical efforts in cluster models [22], the spins and parities of most excited states and their neutron spectroscopic factors are not well determined [23].

In this article, we present the results of studies of $^{11}\text{B}(d, p)$ and $^{12}\text{B}(d, p)$ in inverse kinematics. Section II describes the experimental techniques and results. The deduced spectroscopic factors and neutron-branching ratio of the unbound states are used to estimate the reaction rates of the $^{11}\text{B}(n, \gamma)$ and $^{12}\text{B}(n, \gamma)$ reactions in Sec. III, and the results of $r$-process network calculations with the updated reaction rates are discussed in Sec. IV with a focus on the impact of light, neutron-rich nuclei in heavy-element production. The conclusions are summarized in Sec. V.

## II. EXPERIMENTAL METHODS AND RESULTS

The measurement was performed using the ATLAS facility at Argonne National Laboratory. A radioactive $^{12}\text{B}$ beam was produced using the in-flight method [24] via the $(d, p)$ reaction, by bombarding a deuterium gas cell with an 81-MeV primary $^{11}\text{B}$ beam with an intensity of approximately 100 pnA. The resulting $^{12}\text{B}$ beam had an energy of 75 MeV, was separated from the primary beam using a dipole magnet, and was

delivered to the scattering chamber with an average intensity of $1.2 \times 10^5$ pps.

The experimental setup consisted of a 150 $\mu\text{g/cm}^2$ $\text{CD}_2$ target and three annular double-sided silicon strip detectors (DSSD) for the detection of the protons at backward angles between $110°$ and $161°$ in the laboratory system. The recoiling B ions ($^{11,12,13}\text{B}$) were detected in a telescope of $\Delta E - E$ silicon detectors segmented into four quadrants covering the forward angle range of $1.3° - 7.2°$ in the laboratory system. A silicon surface-barrier-detector telescope was positioned at $0°$ with a mesh attenuator to reduce the direct beam by a factor of 100 to monitor the beam intensity. The DSSDs, with thicknesses of 500 $\mu\text{m}$ each, were segmented into 16 annular rings on the front and 16 azimuthal wedges on the back. The energy resolutions of DSSDs were measured to be 35–45 keV FWHM with $\alpha$ particles from a $^{228}\text{Th}$ source. The forward telescope detector consisted of a 75-$\mu\text{m}$-thick $\Delta E$ detector and a 1000-$\mu\text{m}$ $E$ detector. The setup and the detection technique are described in detail in Ref. [25].

For the radioactive $^{12}\text{B}$ beam, bound and unbound states in $^{13}\text{B}$ are separated by identifying $^{12}\text{B}$ and $^{13}\text{B}$ nuclei in the $\Delta E$-$E$ telescopes. Figures 1(a) and 1(c) show typical particle-identification spectra from $^{11,12}\text{B} + \text{CD}_2$ interactions, respectively. The $^{12,13}\text{B}$ and $^{11,12}\text{B}$ recoil ions are clearly separated. Figures 1(b) and 1(d) show excitation-energy spectra for the $^{11}\text{B}(d, p)^{12}\text{B}$ and $^{12}\text{B}(d, p)^{13}\text{B}$ reactions with selections on the beamlike recoil ions described above. This approach permits a separation of events populating neutron-bound and unbound recoils and permits the determination of branching ratios for neutron and $\gamma$-ray decay.

Considering the larger energy loss and straggling of a beam in a target in inverse kinematics and the 3-mm-diameter spot of the radioactive beam, the overall $Q$-value resolution was approximately 250 keV (FWHM). To optimize this resolution, it was necessary to correct for the azimuthal asymmetry because of small misalignments ($\sim$2 mm) of the DSSD detectors relative to the beam axis. The coincidence efficiency between protons and recoils was obtained from Monte Carlo simulations of the detection setup. These simulations included the realistic detector geometry, nonworking strips, the beam-spot size, and the actual energy thresholds and resolutions for DSSDs obtained from $\alpha$-source calibrations. The final efficiency was calculated for the $d(^{11,12}\text{B}, p)$ reaction and ranged from 40% to 95% for the angles in the center of mass system larger than $10°$. These results were then used to reproduce the $Q$-value resolution of the $d(^{12}\text{B}, p)$ data resulting from the detector angular offsets and beam-spot size. The same analysis algorithm was applied to the simulation and data, verifying the corrections applied for improving the $Q$-value resolution.

### A. $d(^{11}\text{B}, p)^{12}\text{B}$

We obtained angular distributions for states in $^{12}\text{B}$ at $E_X = 0.0, 0.953, 1.674$, and $2.621$ MeV, below the neutron threshold, and for the unbound states at $E_X = 3.389$ and $4.301$ MeV. As shown in Fig. 2, the proton angular distributions for most bound states are well described by distorted-wave Born approximation (DWBA) calculations using the finite-range
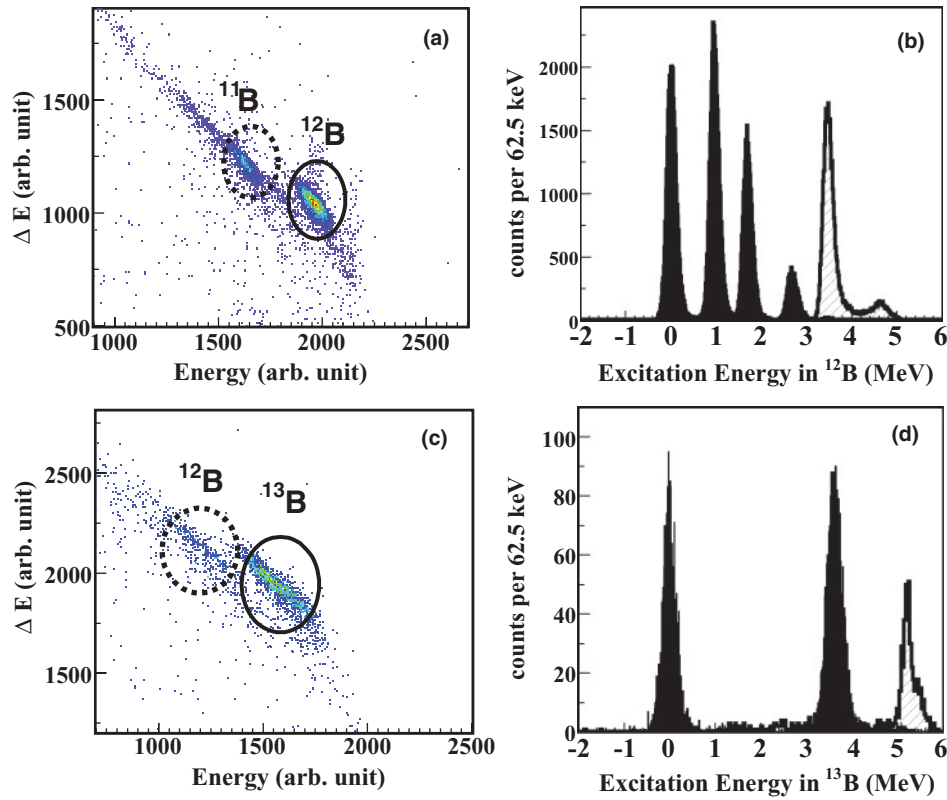
FIG. 1. (Color online) Particle identification spectra with $^{11,12}$B beams. Panels (a) and (c) show plots of $\Delta E$ versus $E$ from the forward recoil detectors and panels (b) and (d) show excitation energy spectra for $^{12}$B and $^{13}$B. The solid histogram in panel (b) is obtained by selecting events within the solid circle in panel (a) (i.e., recoiling $^{12}$B from the $(d,p)$ reaction). The hatched histogram is obtained by selecting events within the dashed circle (i.e., recoiling $^{11}$B from the $(d,p)^{12}$B$(n)^{11}$B). Panels (c) and (d) show the same as described for panels (a) and (b) only for the $^{12}$B beam.

code PTOLEMY [27]. The optical-model parameters for these calculations are summarized in Table I.

The minima in the $\ell = 0$ angular distributions are smeared out by the angular resolution, which is indicated by the horizontal error bars in Fig. 2. For the 1.674-MeV state, the calculated DWBA cross section was also averaged over the same angular bins as the data to check the comparison in the region of the 22° minimum in the calculation (dash-dotted line). The averaging has only a small effect, and the extracted spectroscopic factor is the same as that extracted from the unaveraged curve, within the measurement uncertainty. Also, the doublet at 2.621 and 2.723 MeV was unresolved within our $Q$-value resolution, so the DWBA curve was calculated for the sum of both transitions with previously
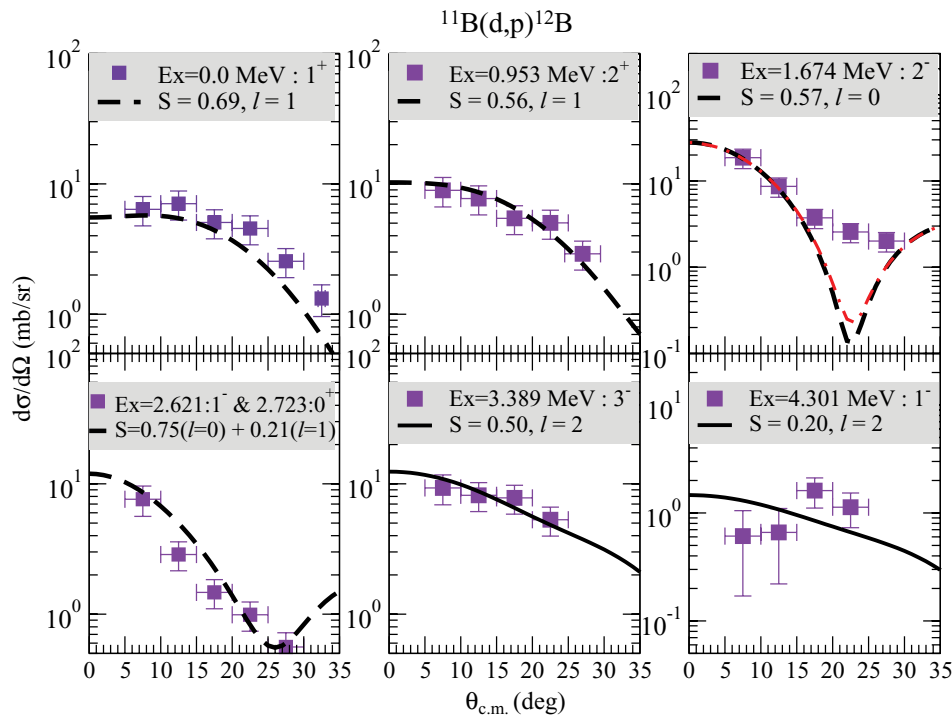


FIG. 2. (Color online) Angular-distribution data for the $^{11}$B$(d,p)^{12}$B reaction in inverse kinematics with the DWBA calculations. The dashed lines correspond to spectroscopic factors from Ajzenberg-Selove [26] and the solid lines are normalized to the current data. See the text for details.

TABLE I. Optical-model parameters used in the DWBA calculations.

| Channel | $V$ (MeV) | $r_0$ (fm) | $a$ (fm) | $W/V_{SO}$ (MeV) | $r_0'$ (fm) | $a'$ (fm) | $r_C$ (fm) | Ref. |
|---|---|---|---|---|---|---|---|---|
| $^{11,12}$B $+ d$ | 81 | 1.15 | 0.81 | 8.6[a] | 1.34 | 0.873 | 1.3 | [28] |
| $^{12,13}$B $+ p$ | 40 | 1.2 | 0.7 | 10.9[a] | 1.2 | 0.46 | 1.3 | [29] |
| $^{11,12}$B $+ n$ | Varied | 1.24 | 0.45 | 5[b] | 1.12 | 0.57 | 1.3 | – |

[a]$(W, r_0', a')$ refer to the surface-derivative imaginary potential.
[b]$(V_{SO}, r_0', a')$ refer to the spin-orbit potential.

determined spectroscopic factors. The spectroscopic factors for bound states agree within 25% with the values from Refs. [26,30] (dashed lines). The spectroscopic factors for the unbound states are estimated with a form factor calculated as though the states are bound at 50 keV. The ratio of the neutron spectroscopic factors between the two unbound states is expected to be the same as their neutron-reduced widths. The spectroscopic factor for the 3.389-MeV state has been previously reported to be 0.57 [31], which is consistent with our value of $0.50 \pm 0.13$.

For the unbound state at 3.389 MeV in $^{12}$B, the partial widths were previously measured to be $\Gamma_n = 3.1 \pm 0.6$ eV and $\Gamma_\gamma = 0.025 \pm 0.008$ eV [32], yielding a ratio of $\Gamma_n / \Gamma_\gamma = 124 \pm 40$. The value from the current measurement, obtained by comparing the proton yields in coincidence with either $^{11}$B recoils (neutron emission) or with $^{12}$B recoils ($\gamma$-ray emission) as illustrated in Fig. 3, is $94 \pm 5$, showing the reduction of the fractional uncertainty by a factor of 6. These experimental values are used to estimate the reaction rates in Sec. III.

### B. $d(^{12}\text{B},p)^{13}\text{B}$

The angular distribution for the $d(^{12}\text{B},p)^{13}\text{B}$ ground-state transition was obtained in the same way as with the $^{11}$B beam. Positive-parity states suggested in Ref. [33] were observed near 3.6 MeV of excitation energy in $^{13}$B, but the members of the expected doublet at $E_X = 3.482$ and 3.681 MeV could not be resolved [see Fig. 1(d)]. Because of their low energies, the energies of protons populating the neutron-unbound 5.105- and 5.388-MeV states were very close to the electronic thresholds of the DSSDs, and the efficiencies and yields for these protons were quite sensitive to these thresholds. Therefore, we have not reported angular distributions for these states.

Figure 4 shows proton angular distributions for the ground state. The spectroscopic factor for the ground state, $S = 0.72$, previously used by Rauscher *et al.* for estimating the reaction rates was based on shell-model predictions [34]. The normalization of the current data to DWBA calculations using the same parameters as Table I yields a value of $1.1 \pm 0.3$. The uncertainty includes the statistical errors, the error in beam-intensity normalization, and systematic uncertainties in the DWBA calculations estimated by using different optical-model parameters.
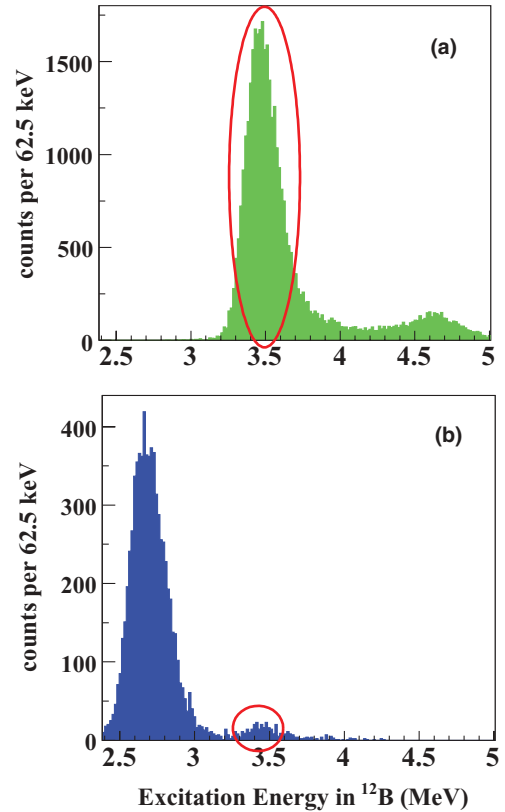


FIG. 3. (Color online) Proton yields from $^{11}$B$(d,p)^{12}$B shown in terms of the excitation energy in $^{12}$B. Panels (a) and (b) show counts in coincidence with $^{11}$B and $^{12}$B, respectively. The neutron threshold is 3.37 MeV and the solid circles highlight the peak corresponding to the unbound 3.389-MeV state, and the yields are integrated over $7°$– $22°$ in the center of mass system.

### III. DETERMINATION OF REACTION RATES

Owing to the low-level density in light nuclei systems, an estimation of the rate for the $(n,\gamma)$ reaction must take into account both nonresonant and resonant captures. The nonresonant capture includes contributions from both direct-capture transitions (DC) and the low-energy tails of giant-dipole resonances at higher energies. For the low-energy neutrons that are most important for $r$-process nucleosynthesis, the electric dipole ($E1$) transition is dominant. The DC cross section for the transition from initial state $i$ to final state $f$ is given [35] as

$$
\sigma_{\text{DC}_{i \to f}}(E1)
$$
$$
= \frac{16\pi}{9} \frac{e_{\text{eff}}^2}{k^2} \frac{k_\gamma^3}{\hbar v} (l_i 010 | l_f 0)^2 \, \text{S}_f \left| \int_0^\infty u_{l_f}(r) \, r \, w_{l_i}(r) dr \right|^2,
$$

$$(1)$$

where $k_\gamma$ is the photon wave-number corresponding to the photon energy $E_\gamma / \hbar c$ and $(....|..)$ is a Clebsch-Gordan coefficient. $w_{l_i}$ represents the continuum states of the target coupled to a neutron and $u_{l_f}$ represents the final bound state with single-particle strength given by $S_f$, the spectroscopic factor. For $s$-wave neutrons, the cross section is proportional to the square of De Broglie wavelength $\lambda$ ($\sim 1/v$) and the
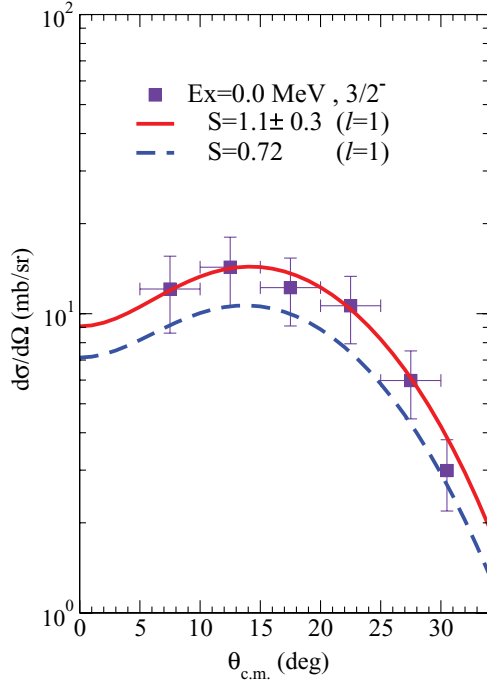
FIG. 4. (Color online) Measured angular distribution for the $^{12}$B$(d,p)^{13}$B reaction compared with the DWBA calculations using the same optical-model parameters as in Table I. Details are discussed in the text.

neutron partial width $\Gamma_n$ ($\sim v$) thus is inversely proportional to the velocity [36]. The reaction rate for low-energy $s$-wave neutrons then may be expressed as

$$N_A \langle \sigma v \rangle_{\text{DC}} = N_A \sigma_T (2kT/\mu)^{1/2}, \qquad (2)$$

where $\mu$ is the reduced mass, and the cross section $\sigma_T$ and the velocity of neutron are obtained at the same temperature $T$. Therefore, the DC reaction rate can be estimated using the available thermal cross section, which was measured with thermal neutrons, and Rauscher $et\ al.$ used this method for the $^{11}$B$(n,\gamma)$ reaction.

For resonant capture, the cross section can be described using the Breit-Wigner formula. The width of the resonance is typically small enough that the Maxwell-Boltzmann velocity distribution inside the integral does not change appreciably, and then the integral of the Breit-Wigner form is given by the resonance strength

$$\omega\gamma = \frac{(2J+1)}{(2J_p+1)(2J_t+1)} \frac{\Gamma_n \Gamma_\gamma}{(\Gamma_n + \Gamma_\gamma)},$$

with $J_p$ ($J_t$) being the spin of the projectile (target) and $\Gamma_n$ ($\Gamma_\gamma$) the partial width for neutron ($\gamma$-ray) decay. The reaction rate is expressed as the sum over for the individual resonance $i$ at the energy $E_i$ as

$$
\begin{aligned}
N_A \langle \sigma v \rangle_r &= 1.54 \times 10^5 \; \mu^{-3/2} T_9^{-3/2} \\
&\quad \times \sum_i \omega\gamma_i \exp\left(-11.605 E_i^{\text{c.m.}}/T_9\right), \qquad (3)
\end{aligned}
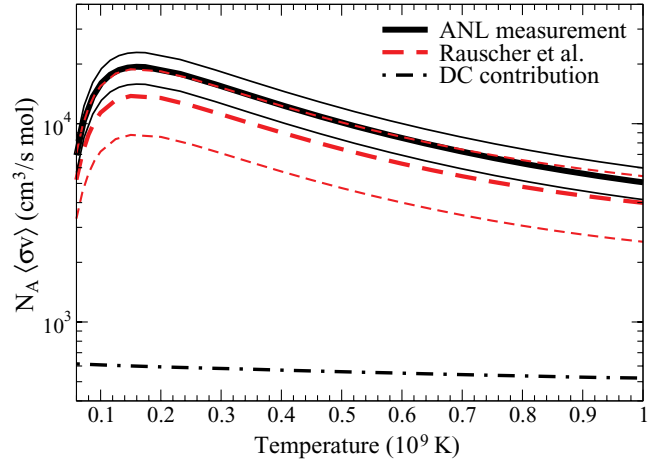$$

where $T_9$ represents the temperature in $10^9$ K.



FIG. 5. (Color online) Total rate for the $^{11}$B$(n,\gamma)$ reaction obtained from the current measurement (the thick solid line) compared with Rauscher's compilation (the thick dashed line). The thin solid and dashed lines are upper and lower limits for the current and Rauscher's rates, respectively. The direct capture contribution is shown by the dashed-dotted line.

For the $^{11}$B$(n,\gamma)$ reaction, the DC cross section was calculated using Eq. (1). We calculated the $s$-wave neutron wave function in the continuum using a Woods-Saxon (WS) potential with a radius of $r_0 = 1.236$ fm and a diffuseness of $d = 0.62$ fm. The potential depth of $V_0 = 56.5$ MeV was obtained by calculating the cross sections for different well depths and then selecting the one that best reproduced the experimental thermal cross section of $\sigma_{\text{th}} = 5.5$ mb [37]. The DC rate is shown by the dashed-dotted line in Fig. 5. The strong resonant contribution at low temperatures is due to the 21-keV unbound state at $E_X = 3.389$ MeV. The smaller branching ratio $(\Gamma_n/\Gamma_\gamma)$ also leads to the larger resonance strength, $\omega\gamma = (3.3 \pm 0.6) \times 10^{-2}$ eV, using the neutron partial width
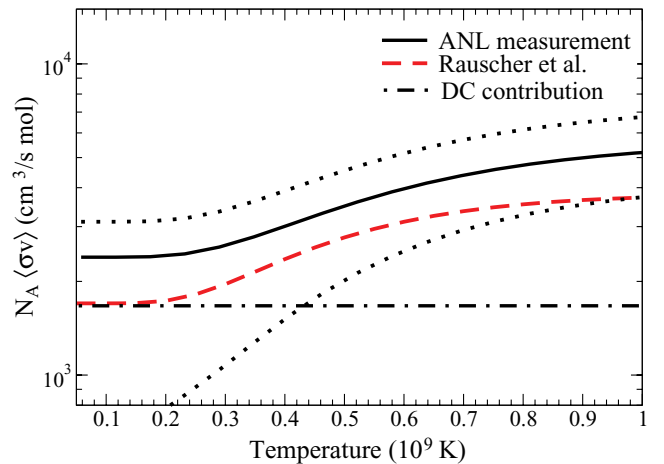


FIG. 6. (Color online) Total rate of the $^{12}$B$(n,\gamma)$ reaction obtained from the current measurement (the thick solid line with upper and lower limits by the dotted lines) compared with the Rauscher's compilation (the dashed line). The direct capture contribution is shown by the dashed-dotted line.
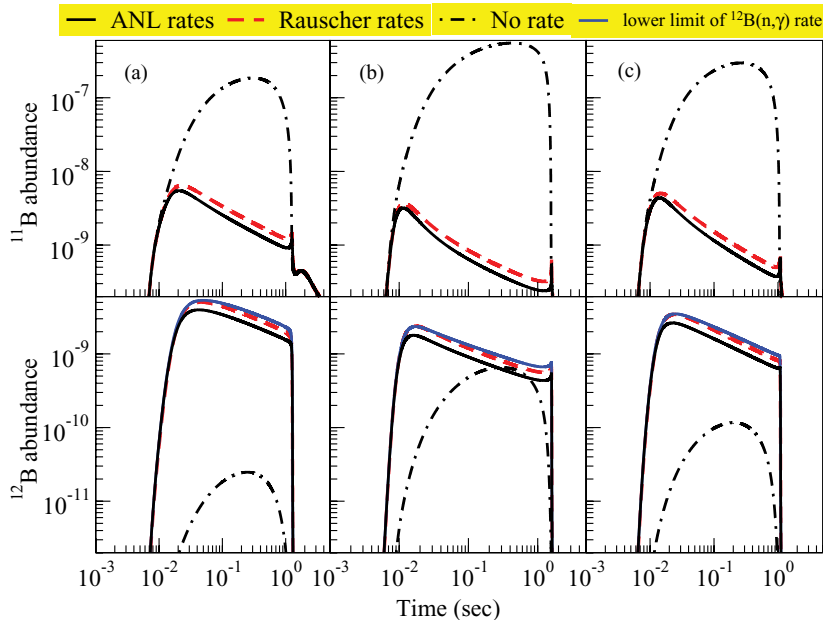
FIG. 7. (Color online) The abundances of $^{11}$B (top) and $^{12}$B (bottom) over time calculated in the $r$-process network using the $^{11,12}$B$(n,\gamma)$ reaction rates from the Rauscher rates (the dashed line) and the ANL rates (the thick solid line). The dashed-dotted line represents the one without including any $^{11,12}$B$(n,\gamma)$ reaction rates and the thin solid line the one using the lower limit of the $^{12}$B$(n,\gamma)$ rate. Different astrophysical conditions of sets (a), (b), and (c) are summarized in Table II.

from Ref. [32]. The final uncertainty includes a 5% contribution from the uncertainty in our measurement and 19% from the neutron partial width reported in Ref. [32]. It is compared to the previous value of $(2.2 \pm 0.8) \times 10^{-2}$ eV [16], which was deduced from the direct measurements of the partial widths [32]. The current data result in an increase of the reaction rate by 50% and a reduction of the uncertainty by a factor of 2 as shown in Fig. 5.

The $^{12}$B$(n,\gamma)$ reaction rate in Ref. [16] was estimated considering $s$-wave direct capture to the ground state and resonant capture to the first two neutron-unbound states at 5.106 and 5.388 MeV. The DC cross section was calculated using first-order perturbation theory [38] and the nuclear correction for the final state was obtained using the calculated spectroscopic factor ($S = 0.72$) [34]. To estimate the reaction rate from our data, we calculated the DC cross section using Eq. (1) (Fig. 6). Because there is no measured thermal cross section on a $^{12}$B target, the WS potential parameters for the $s$-wave neutron wave function were taken from the ones used in the $^{11}$B$(n,\gamma)$ reaction. The bound final state was corrected using our measured spectroscopic factor of $S = 1.1 \pm 0.3$. In contrast to the $^{11}$B$(n,\gamma)$ rate, the resonant capture contributes only at $T_9 > 0.4$, because of the rather high resonance energy ($E_R = 228$ keV) of the first unbound state. As discussed previously in Ref. [39], we also observed a great sensitivity to the choice of the potential depth in calculating the $s$-wave neutron wave function for the $^{12}$B$(n,\gamma)$ reaction and the lower limit of the rate includes this uncertainty. This question could only be answered through a measurement of the neutron scattering on $^{12}$B, which is unfeasible, due to the short lifetime of $^{12}$B.

## IV. ASTROPHYSICAL IMPLICATIONS

Using the updated $^{11,12}$B$(n,\gamma)$ rates from the current measurement (ANL rates), the $r$-process network calculations were performed under different astrophysical conditions as

summarized in Table II. $T_a$ represents the asymptotic temperature, which characterizes how neutrons are consumed during the $r$-process, $S/k$ is the entropy, and $Y_e$ is the initial electron fraction. Sets (a), (b), and (c) were taken from the study of Sasaqui *et al.* [15], as the $^{11}$B$(n,\gamma)$ reaction was expected to have the greatest influence among boron isotopes. Figure 7 compares the abundances of $^{11,12}$B over time using different $^{11,12}$B$(n,\gamma)$ rates. Results using the ANL rates, which are 50% larger than the Rauscher rates, show different $^{12}$B abundances and each parameter set demonstrates different evolutions of the $^{12}$B abundance. The effective temperature for the impact of the ANL rate in $^{12}$B abundances is shown to cover from $T_9 \sim 1.5$ and down to $T_a$ for all four sets.

Figure 8 shows the final $r$-process abundances with two dynamic time scales in the fast steady state wind model, $\tau_{\text{dyn}} = 5$ ms (a, b, c) and $\tau_{\text{dyn}} = 20$ ms (d) using the ANL and Rauscher rates. All the calculations include the effects of fission recycling. Overall, the results from the final abundances are insensitive to the differences in the $(n,\gamma)$ rates, due to such a small variation comparing to the full scale in the change of $^{12}$B abundance. Different astrophysical conditions in sets (a), (b), and (c) yield the different ratios of the second and third $r$-process peaks relative to the first peak. The abundances using the set (d) differ in $A < 75$ and $A > 140$ compared to the other sets, possibly influenced by the lower asymptotic temperature, resulting in a longer $r$-process. As discussed in Ref. [15], the final $r$-process abundances also can strongly be affected by the

TABLE II. Parameter sets used in the fast steady state wind model for the $r$-process calculations.

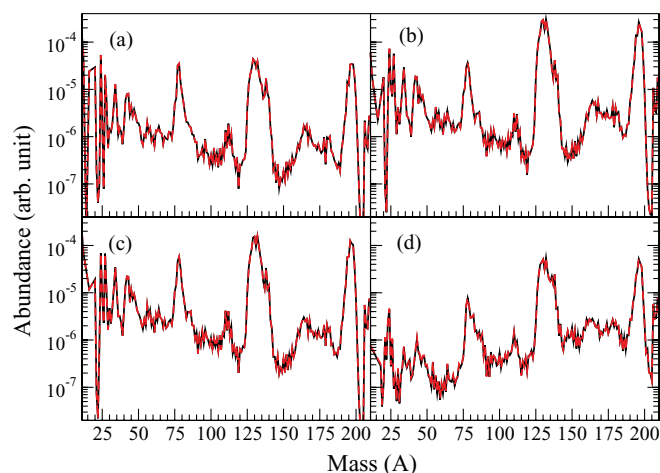| Set | $T_a$ ($10^9$ K) | $\tau_{\text{dyn}}$ (ms) | $S/k$ | $Y_e$ | Ref. [15] |
|-----|------|------|-----|------|-----------|
| (a) | 0.6 | 5 | 350 | 0.45 | Table 10 |
| (b) | 0.6 | 5 | 200 | 0.20 | Table 12 |
| (c) | 0.6 | 5 | 200 | 0.35 | Table 13 |
| (d) | 0.1 | 20 | 250 | 0.45 | — |

FIG. 8. (Color online) Final $r$-process abundances (arb. unit) as a function of mass calculated using the ANL rate (solid line) and the Rauscher rate (dashed line) with the four different astrophysical conditions.

mechanism of supernova explosions, a subject which is still actively under study.

## V. CONCLUSION

The neutron-capture reactions $^{11,12}$B$(n,\gamma)$ were studied indirectly via neutron transfer using the $^{11,12}$B$(d,p)^{12,13}$B reactions in inverse kinematics. The neutron-stripping spectroscopic factors for bound and unbound states in $^{12}$B and $^{13}$B were determined. The branching ratio of the unbound 3.389-MeV state in $^{12}$B was determined directly using the coincidence detection of the ejected proton and the beamlike recoil nuclei. In the present result, the $^{11}$B$(n,\gamma)$ reaction rate is 50% larger, and determined with a reduced uncertainty by a factor of 2, than the previously accepted value. This technique should prove useful for similar determination of the branching ratios, $\Gamma_n/\Gamma_\gamma$, $\Gamma_n/\Gamma_\alpha$, and $\Gamma_n/\Gamma_p$, for the resonance strength in other nuclei at near-threshold states, especially in the cases

where the level density is too small to apply the statistical approach or where measurements of the individual partial widths are unfeasible.

The spectroscopic factor for the ground state of $^{13}$B, which previously has only been estimated from shell-model, was determined to be 50% larger than the calculated value. This increase resulted in an enhancement of the reaction rate of $^{12}$B$(n,\gamma)$, since direct capture dominates the reaction at $T_9 < 1$. The reaction rate of $^{12}$B$(n,\gamma)$ was estimated using experimental information. Studies of resonant and nonresonant captures on these light, neutron-rich nuclei might help us to better understand neutron capture on heavy nuclei far from stability, which have lower level densities and smaller neutron separation energies, and eventually provide better nuclear physics input to predict the $r$-process branching points and the actual $r$-process path.

With several thousands of nuclei involved in the network, our new rates did not show a significant influence on the final abundances from $r$-process nucleosynthesis. We performed the network calculations under different scenarios to improve the understanding of the physical mechanism of supernova explosions and confirmed the importance of sensitivity to the dynamic time scale and the asymptotic temperature. In addition, a recent study of neutrino-induced nucleosynthesis [40] addressed the importance of these neutron-capture reactions on light elements in connection to the weak $r$-process, which could occur at the He-burning shell in core-collapse supernovae. More experimental $(n,\gamma)$ studies up to $T_9 < 2$ with light, neutron-rich nuclei can help to better constrain current astrophysical models. These studies will benefit in the near future from the greater availability of radioactive beams, making possible further systematic measurements on more light, neutron-rich systems.

[1] C. Sneden, J. J. Cowan, I. I. Ivans, G. M. Fuller, S. Burles, T. C. Beers, and J. E. Lawler, Astrophys. J. **533**, L139 (2000).

[2] K.-L. Kratz, K. Farouqi, B. Pfeiffer, J. W. Truran, C. Sneden, and J. J. Cowan, Astrophys. J. **662**, 39 (2007).

[3] S. E. Woosley, J. R. Wilson, G. M. Mathews, R. D. Hoffman, and B. S. Meyer, Astrophys. J. **433**, 229 (1994).

[4] Y.-Z. Qian and S. E. Woosley, Astrophys. J. **471**, 331 (1996).

[5] B. S. Meyer, G. J. Mathews, W. M. Haward, S. E. Woosley, and R. D. Hoffman, Astrophys. J. **399**, 656 (1992).

[6] C. Freiburghaus, S. Rosswog, and F.-K. Thielemann, Astrophys. J. **525**, L121 (1999).

[7] J. C. Wheeler, D. L. Meier, and J. R. Wilson, Astrophys. J. **568**, 807 (2002).

[8] A. G. W. Cameron, Astrophys. J. **587**, 327 (2003).

[9] C. L. Fryer and A. Heger, Astrophys. J. **541**, 1033 (2000).

[10] J. C. Wheeler, I. Yi, P. Hoeflich, and L. Wang, Astrophys. J. **537**, 810 (2000).

[11] J. Pruet, S. E. Woosley, and R. D. Hoffman, Astrophys. J. **586**, 1254 (2003).

[12] S. E. Woosley and R. D. Hoffman, Astrophys. J. **395**, 202 (1992).

[13] K. Otsuki, H. Tagoshi, T. Kajino, and S. Wanajo, Astrophys. J. **533**, 424 (2000).

[14] M. Terasawa, K. Sumiyoshi, T. Kajino, G. J. Mathews, and I. Tanihata, Astrophys. J. **562**, 470 (2001).

[15] T. Sasaqui, T. Kajino, G. J. Mathews, K. Otsuki, and T. Nakamura, Astrophys. J. **634**, 1173 (2005).

[16] T. Rauscher, J. H. Applegate, J. J. Cowan, F.-K. Thielemann, and M. Wiescher, Astrophys. J. **429**, 499 (1994).

[17] F. Ajzenberg-Selove, E. R. Flynn, and O. Hansen, Phys. Rev. C **17**, 1283 (1978).

[18] R. Middleton and D. J. Pullen, Nucl. Phys. **A51**, 50 (1964).

[19] V. Guimarães *et al.*, Phys. Rev. C **61**, 064609 (2000).

[20] S. Ota *et al.*, Phys. Lett. **B666**, 311 (2008).

[21] B. B. Skorodumov *et al.*, Phys. Rev. C **78**, 044603 (2008).

[22] Y. Kanada En'yo, Y. Taniguchi, and M. Kimura, Nucl. Phys. **A805**, 392c (2008).

[23] F. Ajzenberg-Selove, Nucl. Phys. **A523**, 1 (1991).

[24] B. Harss *et al.*, Rev. Sci. Instrum. **71**, 380 (2000).

[25] A. Wuosmaa *et al.*, Phys. Rev. Lett. **94**, 082502 (2005).

[26] F. Ajzenberg-Selove, Nucl. Phys. **A506**, 1 (1990).

[27] M. H. Macfarlane and S. C. Pieper, Argonne National Laboratory Report No. ANL-76-11, 1978.

[28] C. M. Perey and F. G. Perey, Phys. Rev. **132**, 755 (1963).

[29] F. G. Perey, Phys. Rev. **131**, 745 (1963).

[30] J. E. Monahan, H. T. Fortune, C. M. Vincent, and R. E. Segel, Phys. Rev. C **3**, 2192 (1971).

[31] H. T. Fortune and C. M. Vincent, Phys. Rev. **185**, 1401 (1969).

[32] E. F. Mooring, J. E. Monahan, and R. E. Segel, Phys. Rev. **178**, 1612 (1969).

[33] B. A. Brown (private communication).

[34] A. G. M. van Hees and P. W. M. Glaudemans, Z. Phys. A **315**, 223 (1984).

[35] A. M. Lane and J. E. Lynn, Nucl. Phys. **A17**, 563 (1960).

[36] W. A. Fowler, G. R. Caughlan, and B. A. Zimmerman, Annu. Rev. Astron. Astrophys. **5**, 525 (1967).

[37] W. L. Imhof, R. G. Johnson, F. J. Vaughn, and M. Walt, Phys. Rev. **125**, 1334 (1962).

[38] C. Rolfs, Nucl. Phys. **A217**, 29 (1973).

[39] A. Mengoni, T. Otsuka, and M. Ishihara, Phys. Rev. **52**, R2334 (1995).

[40] D. K. Nadyozhin and I. V. Panov, J. Phys. G **35**, 014061 (2008).